Article

Electron Affinities of 1,1-Diaryl-2,3,4,5-tetraphenylsiloles: Direct Measurements and Comparison with Experimental and Theoretical Estimates

Xiaowei Zhan, Chad Risko, Fabrice Amy, Calvin Chan, Wei Zhao,
Stephen Barlow, Antoine Kahn, Jean-Luc Brdas, and Seth R. Marder

J. Am. Chem. Soc., **2005**, 127 (25), 9021-9029• DOI: 10.1021/ja051139i • Publication Date (Web): 04 June 2005

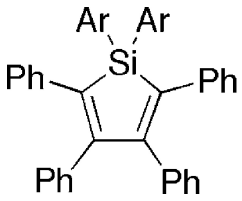

Ar = Ph; 2-(9,9-dimethylfluorenyl); 2-thienyl; C_6F_5

Electron Affinity = -1.5 to -2.4 eV

More About This Article

Additional resources and features associated with this article are available within the HTML version:

- Supporting Information
- Links to the 14 articles that cite this article, as of the time of this article download
- Access to high resolution figures
- Links to articles and content related to this article
- Copyright permission to reproduce figures and/or text from this article

View the Full Text HTML

J|A|C|S
ARTICLES
Published on Web 06/04/2005

Electron Affinities of 1,1-Diaryl-2,3,4,5-tetraphenylsiloles: Direct Measurements and Comparison with Experimental and Theoretical Estimates

Xiaowei Zhan,[†] Chad Risko,[†] Fabrice Amy,[‡] Calvin Chan,[‡] Wei Zhao,[‡] Stephen Barlow,[†] Antoine Kahn,*[,‡] Jean-Luc Brédas,*[,†] and Seth R. Marder*[,†]

Contribution from the School of Chemistry and Biochemistry and the Center for Organic Photonics and Electronics, Georgia Institute of Technology, Atlanta, Georgia 30332, and Department of Electrical Engineering, Princeton University, Princeton, New Jersey 08544

Received February 22, 2005; E-mail: seth.marder@chemistry.gatech.edu

Abstract: We present a comprehensive experimental and theoretical characterization of the electronic structure of four 1,1-diaryl-2,3,4,5-tetraphenylsiloles (aryl = phenyl, 2-(9,9-dimethylfluorenyl), 2-thienyl, pentafluorophenyl). Solid-state electron affinities and ionization potentials of these siloles were measured using inverse-photoelectron spectroscopy (IPES) and photoelectron spectroscopy (PES), respectively; the density of electronic states obtained from calculations performed at the density functional theory (DFT) level corresponds very well to the PES and IPES data. The direct IPES measurements of electron affinity were then used to assess alternative estimates based on electrochemical and/or optical data. We also used DFT to calculate the reorganization energies for the electron-transfer reactions between these siloles and their radical anions. Additionally, optical data and ionization potential and electron affinity data were utilized to estimate the binding energies of excitons in these siloles.

I. Introduction

Siloles (silacyclopentadienes, Figure 1) have recently attracted attention as useful materials for organic electronics since they may exhibit high electron mobilities and high photoluminescence quantum yields. Time-of-flight electron mobilities of **1** were found to be ca. 2×10^{-4} cm^2/Vs, a 2-order of magnitude improvement compared to the well-established electron-transport (ET) material tris(8-hydroquinolinato)aluminum (Alq_3); moreover, the electron transport was shown to be nondispersive and independent of exposure to air.[1−3] Accordingly, siloles have been used as efficient ET materials in organic light-emitting diodes (OLEDs).[4] Furthermore, **2** possesses a photoluminescence (PL) quantum yield of 97 ± 3% in the solid state and has been used as an effective lumophore in OLEDs; for example, an OLED using **2** as an emissive layer and **1** as an ET layer shows a very low operating voltage of 2.5 V and a high external electroluminescence (EL) quantum efficiency of 4.8%.[1] Another EL device based on **3** shows an excellent external EL quantum efficiency of 8%,[5] while **4** has been shown to form a highly emissive exciplex (PL quantum yield of 62%) at the interface with the hole-transport material *N*,*N*′-diphenyl-*N*,*N*′-bis(1-naphthalenyl)-(1,1′-biphenyl)-4,4′-diamine (NPD) and has been exploited in a three-layer device with the configuration Ag:Mg/**1**/**4**/NPD/ITO, which has an external EL quantum efficiency of 3.4%.[6]

In designing organic electronic devices, it is important to be able to assess hole- and electron-injection barriers at the various organic/organic and organic/inorganic interfaces. These are typically estimated by comparing ionization potentials (IPs) and electron affinities (EAs) of the molecular components with each other and/or with the Fermi energies of inorganic electrode materials, respectively.[7] Although approximate IPs and EAs have often been derived from solution electrochemical data, such evaluations require reversible electrochemistry and assume similar solvation effects and solid-state polarization effects on the formation of ions in both the species of interest and the reference compound. The most direct experimental probes of IP and EA are photoelectron spectroscopy (PES) and inverse-photoelectron spectroscopy (IPES), respectively.

Here we report a study of the electronic properties of 1,1-diaryl-2,3,4,5-tetraphenylsiloles. We selected this class of siloles given that: (i) it has previously been reported that OLEDs based on siloles with $R_1 = R_1' =$ Ph are much brighter and more

[†] Georgia Institute of Technology.
[‡] Princeton University.

(1) Murata, H.; Kafafi, Z. H.; Uchida, M. *Appl. Phys. Lett.* **2002**, *80*, 189−191.
(2) Murata, H.; Malliaras, G. G.; Uchida, M.; Shen, Y.; Kafafi, Z. H. *Chem. Phys. Lett.* **2001**, *339*, 161−166.
(3) Mäkinen, A. J.; Uchida, M.; Kafafi, Z. H. *J. Appl. Phys.* **2004**, *95*, 2832−2838.
(4) Tamao, K.; Uchida, M.; Izumizawa, T.; Furukawa, K.; Yamaguchi, S. *J. Am. Chem. Soc.* **1996**, *118*, 11974−11975.
(5) Chen, H. Y.; Lam, W. Y.; Luo, J. D.; Ho, Y. L.; Tang, B. Z.; Zhu, D. B.; Wong, M.; Kwok, H. S. *Appl. Phys. Lett.* **2002**, *81*, 574−576.
(6) Palilis, L. C.; Mäkinen, A. J.; Uchida, M.; Kafafi, Z. H. *Appl. Phys. Lett.* **2003**, *82*, 2209−2211.
(7) This approach overlooks effects such as vacuum-level offsets brought about due to interface dipole formation and effects due to creation of new species with "gap states" close to the interfaces. Indeed, Kafafi and co-workers have found gap states formed at the silole/magnesium interface using PES. However, these effects are likely to be negligible in organic/organic interfaces and will be very material-specific in the case of organic/inorganic interfaces; see ref 3.

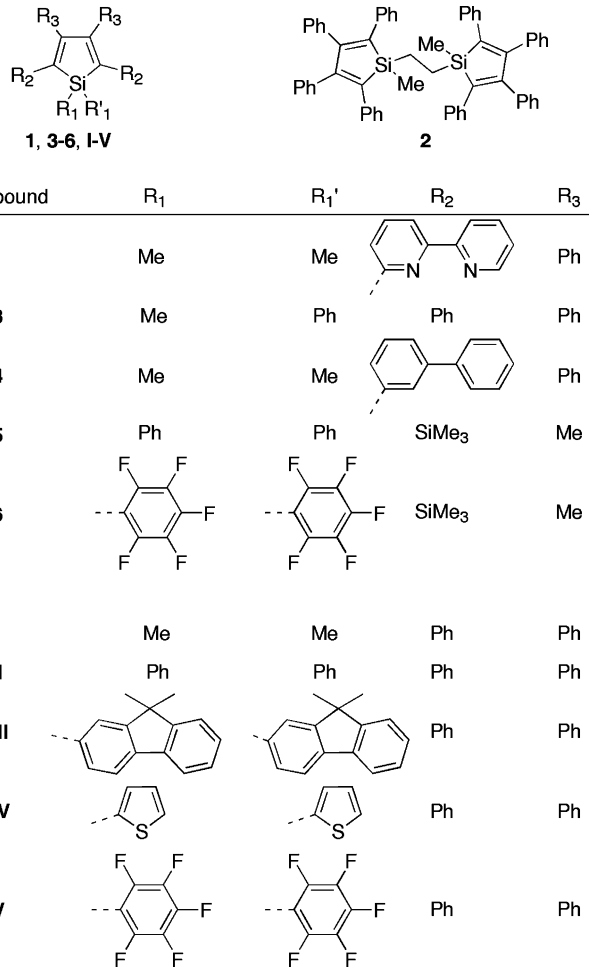

Figure 1. Structures of siloles discussed in this article. **1**−**6** are discussed in the Introduction; **I**−**V** are the species compared in detail in this article.

efficient than those based upon siloles with $R_1 = R_1' =$ alkyl[8] and (ii) thermal stability is an important materials parameter for OLEDs, and 1,1-diaryl siloles have higher melting points and glass-transition temperatures than their 1,1-dialkyl counterparts (see Table S1 in Supporting Information). The electronic effects of 1,1-substituents in siloles have previously been probed by electrochemistry,[9,10] as well as by UV−vis absorption and ab initio calculations;[11] however, there is only one report in which two different aryl groups are compared (**5** versus **6**), and this study only compared UV−vis data.[11] Additionally, despite considerable interest in the ET properties of siloles, no direct measurements of EAs have been published, and only a few studies have involved the determination of an IP (**1**, **2**, **4**) by PES.[3,12,13] To probe the effects of the 1,1-diaryl groups on the electronic structure of the siloles in more detail, we have synthesized three new species where these aryl groups are 2-(9,9-dimethylfluorenyl) (**III**), 2-thienyl (**IV**), or pentafluorophenyl (**V**) and compared them to the previously reported 1,1-diphenyl-2,3,4,5-tetraphenylsilole, **II**, and 1,1-methyl-2,3,4,5-tetraphenylsilole, **I**. As part of this study, we report the first EA measurements for solid-state films of siloles. In addition, we report solid-state IP data, electrochemical data, UV−vis absorption and emission data, and the results of quantum-chemical calculations.

II. Experimental and Theoretical Methodolgy

Synthesis and Characterization. The ^{1}H and ^{13}C NMR spectra were measured on a Varian Mercury 300 spectrometer using tetramethylsilane (TMS; $\delta = 0$ ppm) as an internal standard. Mass spectra were measured on a VG Instruments 70-SE using the electron impact (EI) mode. Elemental analyses were carried out by Atlantic Microlabs using a LECO 932 CHNS elemental analyzer; fluorine analysis was performed by flask combustion followed by ion chromatography. Solution (chloroform, hexane, and toluene) and thin-film (on quartz substrate) UV−vis absorption spectra were recorded on a Varian Cary 5E UV−vis−NIR spectrophotometer, while solution (chloroform) and thin-film PL spectra were recorded on a Shimadzu FP-5301PC spectrofluorometer. Electrochemical measurements were carried out under nitrogen on a deoxygenated solution of tetra-*n*-butylammonium hexafluorophosphate (0.1 M) in 1:1 (by volume) acetonitrile/toluene using a computer-controlled BAS 100B electrochemical analyzer, a glassy-carbon working electrode, a platinum-wire auxiliary electrode, and a Ag wire anodized with AgCl as a pseudo-reference electrode. Potentials were referenced to the ferrocenium/ferrocene ($FeCp_2^{+/0}$) couple by using ferrocene as an internal standard.

Diphenylacetylene, silicon tetrachloride, lithium wire, *n*-butyllithium (1.6 M in hexane), 2-bromofluorene, iodomethane, 2-bromothiophene, bromopentafluorobenzene, and magnesium shavings were purchased from Aldrich and used as received without further purification. 1,1-Dimethyl-2,3,4,5-tetraphenylsilole (**I**) and 1,1-diphenyl-2,3,4,5-tetraphenylsilole (**II**) were prepared according to published procedures.[8]

1,1-Dichloro-2,3,4,5-tetraphenylsilole (VI). This intermediate was prepared according to a procedure reported by Chen et al.[14] Diphenylacetylene (16.8 mmol, 3.0 g) and clean lithium shavings (14 mmol, 98 mg) were put in a 100-mL three-necked round-bottom flask and deoxygenated with nitrogen for 30 min. Dry THF (15 mL) was then added. The reaction mixture was stirred at room temperature for 14 h under nitrogen atmosphere. The resultant deep green mixture was diluted with 50 mL of dry THF and added dropwise to a solution of silicon tetrachloride (6.3 mmol, 1.07 g) in 20 mL of dry THF over a period of 0.5 h at room temperature. The brown mixture was stirred at the same temperature for 2 h and then refluxed for 5 h to give a dark yellow solution. The THF solution of the resultant reactive intermediate **VI** was used in situ for the synthesis of siloles **III**−**V** without isolation.

2-Bromo-9,9-dimethylfluorene (VII). 2-Bromofluorene (160.0 mmol, 39.2 g) was dissolved in 300 mL of DMSO at 60 °C. Potassium iodide (16.0 mmol, 2.7 g) and iodomethane (360.0 mmol, 51.1 g) were then added; finally, powdered potassium hydroxide (640.0 mmol, 36.0 g) was slowly added. The mixture was stirred at room temperature overnight. The mixture was dropped into 2000 mL of water, and a large amount of light yellow precipitate formed. The solid was filtered, washed with water, and dried under vacuum. The light yellow solid was purified by recrystallization from methanol to give white crystals (40.3 g, 92%). mp: 56 °C. ^{1}H NMR (300 MHz, $CDCl_3$): δ 7.72−7.65 (m, 1H), 7.60−7.54 (m, 2H), 7.48−7.39 (m, 2H), 7.37−7.30 (m, 2H), 1.47 (s, 6H). ^{13}C NMR (75 MHz, $CDCl_3$): δ 155.63, 153.19, 138.18, 138.11, 130.04, 127.63, 127.14, 126.12, 122.62, 121.36, 120.98, 120.03, 47.07, 26.98. HRMS (EI): *m*/*z* 272.0197 (calcd for $C_{15}H_{13}Br$, 272.0201). Anal. Calcd for $C_{15}H_{13}Br$: C, 65.95; H, 4.80. Found: C, 65.96; H, 4.80.

(8) Tang, B. Z.; Zhan, X. W.; Yu, G.; Lee, P. P. S.; Liu, Y. Q.; Zhu, D. B. *J. Mater. Chem.* **2001**, *11*, 2974−2978.
(9) Dhiman, A.; Zhang, Z. R.; West, R.; Becker, J. Y. *J. Electroanal. Chem.* **2004**, *569*, 15−22.
(10) Ferman, J.; Kakareka, J. P.; Klooster, W. T.; Mullin, J. L.; Quattrucci, J.; Ricci, J. S.; Tracy, J. J.; Vining, W. J.; Wallace, S. *Inorg. Chem.* **1999**, *38*, 2464−2472.
(11) Yamaguchi, S.; Jin, R. Z.; Tamao, K. *J. Organomet. Chem.* **1998**, *559*, 73−80.
(12) Mäkinen, A. J.; Uchida, M.; Kafafi, Z. H. *Appl. Phys. Lett.* **2003**, *82*, 3889−3891.
(13) Palilis, L. C.; Mäkinen, A. J.; Murata, H.; Uchida, M.; Kafafi, Z. H. *Proc. SPIE* **2003**, *4800*, 256−270.
(14) Chen, J.; Law, C. C. W.; Lam, J. W. Y.; Dong, Y.; Lo, S. M. F.; Williams, I. D.; Zhu, D.; Tang, B. Z. *Chem. Mater.* **2003**, *15*, 1535−1546.

1,1-Bis(9,9-dimethylfluoren-2-yl)-2,3,4,5-tetraphenylsilole (III). To a 250-mL three-necked round-bottom flask were added **VII** (9.5 mmol, 2.6 g) and 20 mL of dry diethyl ether; the solution was deoxygenated with nitrogen for 30 min and cooled to −78 °C. *n*-BuLi (9.6 mmol, 6 mL, 1.6 M) in hexane was dropwise added over a period of 10 min. The mixture was stirred at the same temperature for 1 h to give a white suspension. The THF solution of **VI** was cooled to 0 °C and transferred portionwise into the above organolithium suspension over a period of 30 min. The brown mixture was stirred for 1 h at −78 °C and was gradually warmed to room temperature; the solution was stirred overnight. The resulting yellow-green solution was washed with water; the organic layer was extracted with ether and dried over anhydrous $MgSO_4$. The solvent was removed, and the residue was purified by flash column chromatography over silica gel using hexane/dichloromethane = 8/1 as eluent. Recrystallization from ethanol gave faintly greenish-yellow and highly blue fluorescent crystals (1.6 g, 44%, based on 2-bromo-9,9-dimethylfluorene). mp: 202 °C. ^{1}H NMR (300 MHz, $CDCl_3$): δ 7.77−7.65 (m, 8H), 7.44 (m, 2H), 7.35 (m, 4H), 7.07−6.88 (m, 20H), 1.40 (s, 12H). ^{13}C NMR (75 MHz, $CDCl_3$): δ 156.08, 153.68, 152.86, 141.02, 139.95, 139.72, 138.81, 138.58, 134.70, 131.28, 130.50, 130.19, 129.93, 129.18, 127.65, 127.33, 126.89, 126.45, 126.27, 125.50, 122.58, 120.24, 119.82, 46.82, 26.97. HRMS (EI): *m*/*z* 770.3332 (calcd for $C_{58}H_{46}Si$, 770.3369). Anal. Calcd for $C_{58}H_{46}Si$: C, 90.34; H, 6.01. Found: C, 89.96; H, 5.95. UV ($CHCl_3$), λ_{max} (ϵ_{max}) 278 (5.38×10^4), 311 (5.49×10^4), 368 (0.76×10^4) nm (mol^{-1} L cm^{-1}).

1,1-Bis(thien-2-yl)-2,3,4,5-tetraphenylsilole (IV). To a 250-mL three-necked round-bottom flask were added 2-bromothiophene (12.6 mmol, 2.06 g) and 20 mL of dry diethyl ether; the solution was deoxygenated with nitrogen for 30 min and cooled to −78 °C. A quantity of 7.9 mL of a 1.6 M hexane solution of *n*-butyllithium (12.6 mmol) was added dropwise. The mixture was stirred at the same temperature for 1 h. The THF solution of **VI** was cooled to 0 °C and transferred portionwise into 2-thienyllithium over a period of 30 min. The brown mixture was stirred for 1 h at −78 °C, gradually warmed to room temperature, and stirred overnight. The resulting dark yellow-green solution was washed with water; the organic layer was extracted with diethyl ether and dried over anhydrous magnesium sulfate. The solvent was removed, and the residue was purified by flash column chromatography over silica gel using hexane/dichloromethane = 4/1 as eluent. Recrystallization from ethanol gave faintly greenish-yellow and highly blue fluorescent crystals (1.4 g, 41%, based on silicon tetrachloride). mp: 212 °C. ^{1}H NMR (300 MHz, $CDCl_3$): δ 7.71 (d, J = 4.20 Hz, 2H), 7.51 (d, J = 3.30 Hz, 2H), 7.23 (dd, J = 3.60, 3.30 Hz, 2H), 7.10−6.93 (m, 14H), 6.93−6.80 (m, 6H). ^{13}C NMR (75 MHz, $CDCl_3$): δ 156.37, 138.74, 138.42, 133.10, 129.90, 129.61, 129.45, 128.54, 127.78, 127.47, 126.53, 125.88. HRMS (EI): *m*/*z* 550.1208 (calcd for $C_{36}H_{26}S_2Si$, 550.1245). Anal. Calcd for $C_{36}H_{26}S_2Si$: C, 78.50; H, 4.76; S, 11.64. Found: C, 78.30; H, 4.83; S, 11.46. UV ($CHCl_3$), λ_{max} (ϵ_{max}) 242 (4.03×10^4), 372 (0.80×10^4) nm (mol^{-1} L cm^{-1}).

1,1-Bis(pentafluorophenyl)-2,3,4,5-tetraphenylsilole (V). To a 250-mL three-necked round-bottom flask were added magnesium shavings (25 mmol, 0.6 g), bromopentafluorobenzene (12.6 mmol, 3.11 g), and a little iodine, and these were deoxygenated with nitrogen for 30 min. A quantity of 30 mL of dry THF was added, and the mixture was stirred at 40 °C for 2 h. The gray Grignard reagent suspension was cooled to 0 °C and transferred portionwise into the THF solution of **VI** over a period of 30 min. The brown mixture was stirred for 1 h at 0 °C, gradually warmed to room temperature, and stirred overnight. The resulting dark yellow-green solution was washed with water, and the organic layer was extracted with ether and dried over anhydrous $MgSO_4$. The solvent was removed, and the residue was purified by flash column chromatography over silica gel using hexane/dichloromethane = 2/1 as eluent and recrystallized from acetonitrile to afford yellow-green and highly green fluorescent crystals (2.1 g, 46%, based on silicon tetrachloride). mp: 190 °C. ^{1}H NMR (300 MHz, $CDCl_3$): δ 7.12−6.96 (m, 12H), 6.94−6.80 (m, 8H). ^{13}C NMR (75 MHz, $CDCl_3$): δ 157.78, 151.00 (dm, J_{CF} = 246 Hz, C_6F_5), 144.89 (dm, J_{CF} = 259 Hz, C_6F_5), 139.19 (dm, J_{CF} = 257 Hz, C_6F_5), 137.89, 136.68, 134.78, 129.57, 129.15, 128.01, 127.76, 127.11, 126.68, 103.76 (m, C_6F_5). HRMS (EI): *m*/*z* 718.1191 (calcd for $C_{40}H_{20}F_{10}Si$, 718.1175). Anal. Calcd for $C_{40}H_{20}F_{10}Si$: C, 66.85; H, 2.81; F, 26.44. Found: C, 66.77; H, 2.84; F, 26.25. UV ($CHCl_3$), λ_{max} (ϵ_{max}) 239 (1.45×10^4), 376 (0.38×10^4) nm (mol^{-1} L cm^{-1}).

PES and IPES Data Collection. The PES and IPES measurements were performed in a multichamber ultrahigh vacuum system comprising a growth chamber with organic evaporation stations and quartz-crystal flux monitor connected to a surface analysis chamber equipped with PES and IPES. The four materials were loaded in separate PBN crucibles in the growth chamber. The substrates were Si wafers covered with a 50 Å Ti layer (for adhesion) and a 1200 Å Au layer. Prior to insertion in a vacuum, the substrates were degreased by being boiled in trichloroethylene and rinsed in acetone and methanol. Silole films with thickness ranging from 20 to 50 Å were deposited on the Au surface at a rate of 1 Å/s (assuming a density of 1.5 g/cm^3) and transferred to the analysis chamber. PES was performed using the standard He I (21.22 eV) and He II (40.8 eV) photon lines from a He discharge lamp and a cylindrical mirror analyzer, giving an experimental resolution of 150 meV. IPES was carried out in the isochromat mode using a fixed-photon-energy detector centered at 9.2 eV[15] and a Kimbal Physics electron gun, giving a combined resolution of 500 meV. The IPES electron-beam current density was limited to 1 μA/cm^2 to minimize degradation of the organic material. In all cases, PES was carried out first on the fresh film and repeated after the IPES measurement to assess electron-beam-induced degradation. The PES and IPES energy scales were aligned by measuring the position of the Fermi level of a freshly evaporated Au film. The position of the vacuum level at the surface of each film, E_{vac}, was measured using the onset of photoemission[16] to determine IP and EA. In accord with the ad hoc procedure widely accepted in the literature,[17] the experimental values of adiabatic IP and EA were taken as the energy difference between E_{vac} and the *leading edge* of the HOMO and LUMO feature, respectively.

Computational Details. The geometries of **I**−**V** were optimized in the neutral, radical-anion, and radical-cation states via density functional theory (DFT). The DFT calculations were carried out using the B3LYP functional, where Becke's three-parameter hybrid exchange functional is combined with the Lee−Yang−Parr correlation functional,[18−20] with a 6-31G* split valence plus polarization basis set. Excitation energies for the low-lying excited states were calculated with time-dependent density functional theory (TD-DFT). Simulation of the PES and IPES spectra was accomplished through the density of states (DOS) given by the DFT methodology. To account for polarization effects in the solid state, the DOS was rigidly shifted with respect to the binding-energy axis;[21] the DOS was convoluted with Gaussian functions characterized by a full width at half-maximum (fwhm) of ca. 0.5−0.7 eV to replicate the experimental line widths. Since the B3LYP functional contains correlation effects, neither compression nor expansion of the DOS was performed, in contrast to previous Hartree−Fock-based simulations of PES and IPES data.[22] All DFT calculations were performed with Gaussian98 (revision A.11).[23]

(15) Wu, C. I.; Hirose, Y.; Sirringhaus, H.; Kahn, A. *Chem. Phys. Lett.* **1997**, *272*, 43−47.
(16) Cahen, D.; Kahn, A. *Adv. Mater.* **2003**, *15*, 271−277.
(17) Shen, C.; Kahn, A.; Hill, I. G. In *Conjugated polymer and molecular interfaces: science and technology for photonic and optoelectronic applications*; Salaneck, W. R., Seki, K., Kahn, A., Pireaux, J. J., Eds.; Marcel Dekker: New York, 2002.
(18) Becke, A. D. *Phys. Rev. A* **1988**, *38*, 3098−3100.
(19) Becke, A. D. *J. Chem. Phys.* **1993**, *98*, 5648−5652.
(20) Lee, C.; Yang, W.; Parr, R. G. *Phys. Rev. B* **1988**, *37*, 785−789.
(21) The rigid shifts required for the fitting of the PES/IPES spectra using the DFT DOS were as follows: **II**, 2.97 eV PES, 5.22 eV IPES; **III**, 2.04 eV PES, 5.16 eV IPES; **IV**, 2.79 eV PES, 4.64 eV IPES; and **V**, 2.83 eV PES, 5.20 eV IPES.
(22) Hill, I. G.; Kahn, A.; Cornil, J.; dos Santos, D. A.; Brédas, J. L. *Chem. Phys. Lett.* **2000**, *317*, 444−450.

Scheme 1. Synthetic Routes to Siloles **III**, **IV**, and **V**

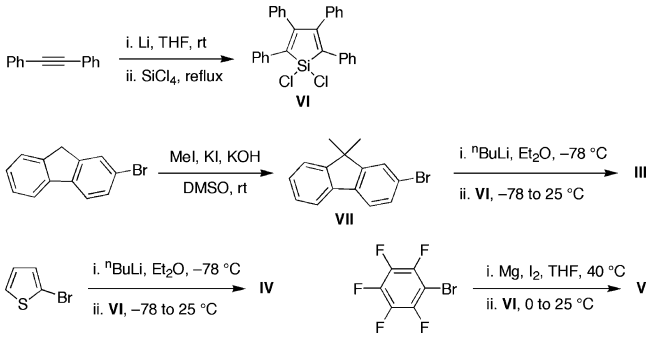

III. Results and Discussion

Synthesis. 1,1-Dimethyl-2,3,4,5-tetraphenylsilole (**I**) and 1,1-diphenyl-2,3,4,5-tetraphenylsilole (**II**) were prepared according to published procedures[8] from the ring-closing reaction of 1,4-dilithio-1,2,3,4-tetraphenyl-1,3-butadiene with dichlorodimethylsilane or dichlorodiphenylsilane, respectively. The new compounds **III**−**V** were made by quenching the same organolithium reagent with silicon tetrachloride to afford the known 1,1-dichlorosilole intermediate, **VI**. **VI** was then transformed to siloles **III**, **IV**, and **V** by the reactions with Grignard or lithium reagents, as shown in Scheme 1. All siloles were prepared in 40−50% yields. All silole products were fully characterized by spectroscopic methods and elemental analysis.

IP and EA Measurements and Simulations. The most direct probes of the energies of filled and empty orbitals of molecules are PES and IPES, respectively. Data were acquired on vapor-deposited thin films of the 1,1-diaryl-substituted siloles, **II**−**V**,[24] since these data are more relevant to device applications. It should be noted that experimental thin-film IPs for small molecules have previously been shown to be as much as 1−1.5 eV lower than the experimental gas-phase values due to extra stabilization of the cation in the solid state through polarization of the surrounding medium;[25−27] accordingly, EA values are expected to be more exothermic in the solid state than the gas phase due to polarization stabilization of the anion.[28] The spectra are shown in Figure 2, along with simulations based upon DFT calculations that facilitate interpretation and assignment of the spectra; it should be noted that few such comparisons between theoretical and experimental densities of states of *both* filled and empty orbital structures have been published.[22] The experimentally determined IPs and EAs are given in Table 1. These estimates of the adiabatic values are obtained from the onsets of the spectra, the relatively large error bars at least partially stemming from difficulties associated with accurate determinations of these onsets. The adiabatic and vertical gas-phase IPs/EAs from DFT self-consistent-field calculations are included for comparison. The absolute experimental values are not expected to agree with those calculated, since the calculations neglect solid-state polarization effects; thus, the apparent close similarity between calculated gas-phase and experimental thin-film IP values is an adventitious artifact of the computational methodology used. The experimental IPs fall in the range 6.05−6.78 eV, considerably higher than the solid-state IP values for typical hole-transport (HT) materials such as *N*,*N*′-diphenyl-*N*,*N*′-di(3-methylphenyl)-(1,1′-biphenyl)-4,4′-diamine (TPD) (5.38 eV, adiabatic) and NPD (5.5 eV[29,30]), suggesting a high barrier for hole injection into the siloles from these materials. The EAs (−1.5 to −2.4 eV) may be compared to a value in the range −2.0 to −2.5 eV measured for the widely used ET material, Alq_3.[16] This suggests that electron-injection barriers similar to those obtained with Alq_3 could be realized with some of these siloles. The experimental IP and EA values for **II**, **III**, and **IV** are close, within experimental error, whereas **V** is harder to oxidize and easier to reduce than **II**−**IV**. The DFT calculations reproduce this pattern.

The calculated HOMOs and LUMOs (experimentally probed by the PES and IPES measurements, respectively) for **II**−**V** do not vary drastically in appearance among the different compounds; moreover, they are similar to those reported in other computational studies of siloles.[10,11,31] The HOMO is similar to the Hückel HOMO for *cisoid*-butadiene, with some additional antibonding contributions from the local HOMOs of 2,5- and, to a lesser extent, 3,4-phenyl groups; see Figure 3. The LUMO resembles the LUMO of butadiene with additional in-phase contributions from a Si−Ar σ^* orbital and from the local LUMOs of the 2,3,4,5-phenyl groups. Significantly, neither HOMO nor LUMO shows any obvious contributions from the π-orbitals of the 1,1-diaryl groups; thus, the variation of the substituents on silicon appears to affect the electronic structure through a principally inductive mechanism. While this has been proposed in previous studies,[11] it has also been suggested that when the 1,1-substituents are phenyl, π-effects are important.[11] However, support for a mainly inductive role of the aryl groups comes from the similar effects of a given substituent on both HOMO and LUMO energies (see Table S2 in Supporting Information). Moreover, the computed IP and EA data suggest slightly lower-lying HOMO and LUMO for the thienyl species, **IV**; although thiophene is an electron-rich π-system, it has previously been shown that the 2-thienyl group is inductively somewhat electron-withdrawing.[32]

Electrochemistry. Since cyclic voltammetry is a much more routine experiment than either PES or IPES, we were interested in establishing the extent to which the trends seen in PES and IPES, and in the calculations, could be discerned from electrochemical data. Moreover, it is of interest to compare how IP and EA energies estimated from the electrochemical data compare with those determined more directly by PES and IPES. An example of a cyclic voltammogram is illustrated in Figure 4. The siloles **I**−**V** show one (**II**−**V**) or two (**I**) oxidation peaks and two reduction peaks, none of which appears fully reversible, indicating the charged species to be unstable in solution; the anodic peak potentials, E_{pa}, and cathodic peak potentials, E_{pc}, are summarized in Table 2. Due to the incomplete reversibility of these processes, the peaks do not necessarily represent the

(23) Frisch, M. J. et al. *Gaussian98*, revision A.11; Gaussian, Inc.: Pittsburgh, PA, 1998.
(24) We were unable to acquire spectra for **I** for comparison since **I** was too volatile under the high-vacuum conditions required for the spectroscopy.
(25) Anderson, J. D. et al. *J. Am. Chem. Soc.* **1998**, *120*, 9646−9655.
(26) Sato, N.; Inokuchi, H.; Silinsh, E. A. *Chem. Phys.* **1987**, *115*, 269−277.
(27) Silinsh, E. A.; Capek, V. *Organic Molecular Crystals: Interaction, Localization, and Transport Phenomena*; AIP Press: New York, 1994.
(28) Interestingly, computationally estimated polarization energies for anthracene are similar for both holes and electrons, whereas for perylene tetracarboxylic acid dianhydride they differ by more than 2 eV (Tsiper, E. V.; Soos, Z. G. *Phys. Rev. B* **2001**, *64*, 195124−1−195124−12).
(29) Kahn, A.; Koch, N.; Gao, W. Y. *J. Polym. Sci., Part B: Polym. Phys.* **2003**, *41*, 2529−2548.
(30) Gao, W. Y.; Kahn, A. *J. Appl. Phys.* **2003**, *94*, 359−366.
(31) Risko, C.; Kushto, G. P.; Kafafi, Z. H.; Brédas, J. L. *J. Chem. Phys.* **2004**, *121*, 9031−9038.
(32) Fringuel, F.; Marino, G.; Taticchi, A. *J. Chem. Soc. B* **1971**, 2302−2303.

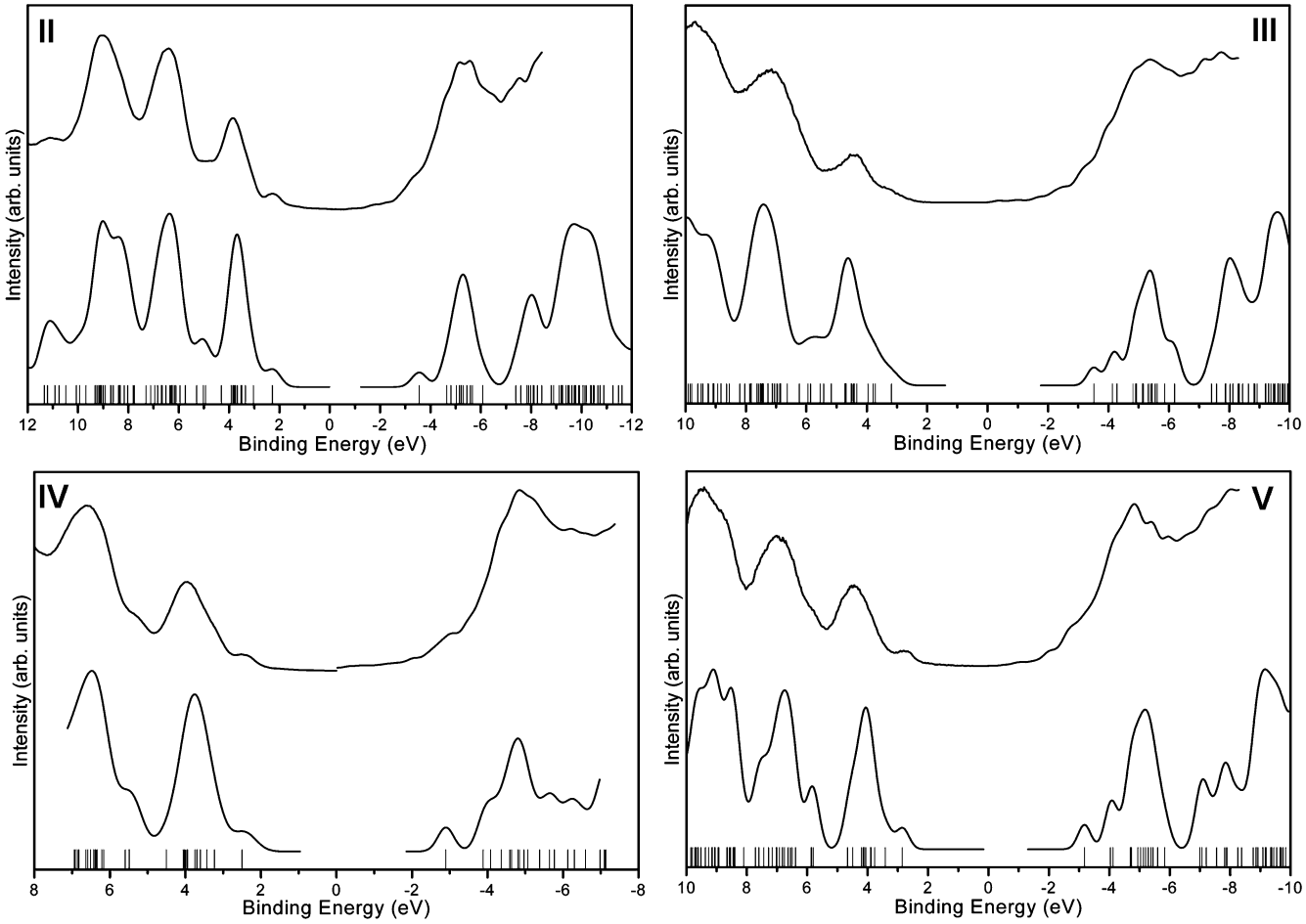

Figure 2. Comparison between PES and IPES spectra measured for **II**−**V**. For each compound, the thin-film (top) and DFT-simulated (bottom) spectra are given; the vertical bars refer to the shifted energies of the molecular orbitals.

Table 1. Experimental PES and IPES Estimates of Thin-Film Adiabatic IP and EA (eV, from Onset) and DFT Calculations of Gas-Phase Adiabatic and Vertical IP and EA

	IP			EA		
	PES	DFT		IPES	DFT	
		adiabatic	vertical		adiabatic	vertical
I	−	6.30	6.54	−	−0.62	−0.34
II	6.19 ± 0.10	6.19	6.42	−1.85 ± 0.40	−0.78	−0.52
III	6.40 ± 0.10	6.10	6.29	−1.49 ± 0.40	−0.83	−0.58
IV	6.05 ± 0.10	6.23	6.46	−1.93 ± 0.40	−0.85	−0.58
V	6.78 ± 0.10	6.49	6.85	−2.41 ± 0.40	−1.16	−0.86

thermodynamic oxidation and reduction potentials and should be interpreted with caution. However, the electrochemical data do reveal a picture similar to that of the PES and IPES data: **II**−**IV** are similar to one another in IP and EA, with **V** both significantly easier to reduce and harder to oxidize than **I**−**IV**. The differences in the electrochemical data are less pronounced than those in the experimental and calculated IP and EA data, presumably due to differences in solvation effects. These results are consistent with previous cyclic voltammetry studies upon the influence of 1,1-substituents in which Dhiman and co-workers reported that siloles with electron-withdrawing 1,1-substituents (e.g., chlorine) show higher first oxidation potentials.[9]

The solid-state IP of a molecular species is often estimated from comparison of the electrochemical potential for the $M^{+/0}$ couple with that for a compound whose solid-state IP has been

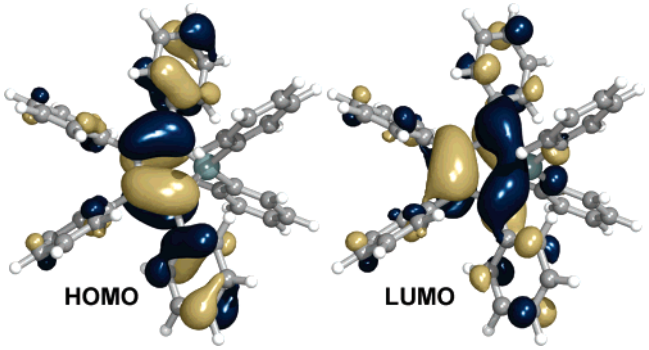

Figure 3. B3LYP/6-31G*-calculated highest occupied (HOMO) (left) and lowest unoccupied (LUMO) (right) one-electron molecular orbitals for **II**.

determined by PES (e.g., the commonly used hole-transport molecule TPD). From the electrochemical data, one would then estimate the IP of **I**−**V** to be in the range ca. 6.0−6.2 eV (ca. 6.1 eV for **II**) using the relation

$$\mathrm{IP(M)} - \mathrm{IP(TPD)} = E_{1/2}(\mathrm{M}^{+/0}) - E_{1/2}(\mathrm{TPD}^{+/0})$$

with values of 5.38 eV for the IP of TPD (thin film) and +0.35 V for $E_{1/2}(\mathrm{TPD}^{+/0})$ (in MeCN/benzene),[25] and assuming $E_{1/2}$ is similar to E_{pa1}. These values are of similar magnitude to those from PES (6.05−6.78 eV), although the range of values seen in PES is considerably reduced in the electrochemical data and the value for **V** is significantly underestimated.

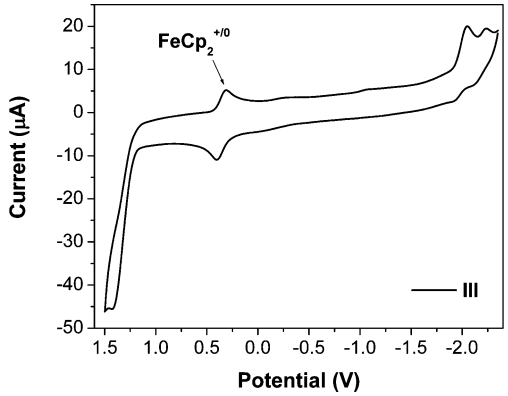

Figure 4. Cyclic voltammogram of silole **III** (with $FeCp_2$ as an internal reference) in CH_3CN/toluene (1:1 volume)/0.1 M $[^nBu_4N]^+[PF_6]^-$ at 50 mVs^{-1}. The horizontal scale refers to an anodized Ag wire pseudo-reference electrode.

Table 2. Electrochemical Data (V) for **I**−**V**[a]

	E_{pa1}[b]	E_{pa2}[b]	E_{pc1}[b]	E_{pc2}[b]
I	+0.95	+1.10	−2.43	−2.84
II	+1.02	−	−2.35	−2.57
III	+1.07	−	−2.41	−2.60
IV	+1.05	−	−2.25	−2.48
V	+1.17	−	−2.08	−2.40

[a] In CH_3CN/toluene (1:1 volume)/0.1 M $[^nBu_4N]^+[PF_6]^-$, versus ferrocenium/ferrocene at 50 mVs^{-1}. [b] E_{pa1} and E_{pa2} are the peak potentials corresponding to successive molecular oxidations, while E_{pc1} and E_{pc2} are the peak potentials corresponding to successive molecular reductions.

EAs can, in principle, be estimated according to:

$$\mathrm{EA(M)} + \mathrm{IP(TPD)} = E_{1/2}(\mathrm{TPD}^{+/0}) - E_{1/2}(\mathrm{M}^{0/-})$$

For **II**, a value of ca. −2.7 eV is estimated, suggesting injection of an electron into the solid to be almost 1 eV easier than is indicated by the IPES data. This poor agreement with the IPES value can be attributed to different magnitudes of solvation effects and polarization effects on $E_{1/2}$ and IP/EA, respectively; solvation appears to stabilize TPD^+ and/or M^- more than solid-state effects. An alternative estimate of the EA that is often used is to combine the IP and the optical gap, E_{op} (estimated 0−0 transition, vide infra), according to:

$$\mathrm{EA} = E_{op} - \mathrm{IP}$$

For **II**, a value of ca. −3.2 to −3.1 eV is obtained (using either the PES or the electrochemical estimate of IP), also more than 1 eV different from the IPES value. This method has also been previously used to estimate similar values for the EA of siloles (**1**, **2**, **4**) from PES-determined IPs.[13] The poor agreement with the IPES value of EA using this method is largely attributable to the neglect of the exciton-binding energy (vide infra).

An alternative electrochemical estimate of EA can be obtained from comparison to a material of known EA and reduction potential, such as Alq_3, via:

$$\mathrm{EA(M)} - \mathrm{EA}(Alq_3) = E_{1/2}(Alq_3^{0/-}) - E_{1/2}(\mathrm{M}^{0/-})$$

Taking $E_{1/2}(Alq_3^{0/-}) = -2.30$ V,[25] this method suggests that the EA for **II** is close to that for Alq_3 (−2.0 to −2.5 eV[16]), closer to the values from IPES data than those estimated above. While the large uncertainties in the present IPES EA values and in that for Alq_3 preclude detailed comparison of the electrochemically estimated and IPES values of EA, it does seem that EA energies are best estimated from comparison of $E_{1/2}(M^{0/-})$ values with that of a compound of known EA, whereas IP energies are best estimated from comparison of $E_{1/2}(M^{+/0})$ values with that of a compound of known IP.

Table 3. B3LYP/6-31G* Intramolecular Reorganization Energies as Determined by ΔSCF[a]

	neutral/cation			neutral/anion		
	λ_1 (eV)	λ_2 (eV)	λ_{total} (eV)	λ_1 (eV)	λ_2 (eV)	λ_{total} (eV)
I[b]	0.21	0.24	0.45	0.24 *0.22*	0.27 *0.28*	0.51 *0.50*
II	0.20	0.22	0.42	0.23	0.26	0.49
III	0.19	0.19	0.38	0.24	0.26	0.50
IV	0.21	0.23	0.44	0.24	0.27	0.51
V	0.25	0.36	0.61	0.26	0.30	0.56

[a] The total intramolecular reorganization energy (λ_{total}) combines the relaxation energies of the initially neutral molecule (λ_1) and the initially ionized molecule (λ_2) upon electron transfer (polaron hopping). [b] For **I**, values in italics were determined by vibrational mode analysis.

Reorganization Energies. Since siloles can show moderate electron mobilities in excess of that seen for Alq_3, we were interested in comparing the barriers to electron transfer between anionic and neutral species in the two systems; according to Marcus theory,[33−35] the barrier height, $\Delta G^{\ddagger}$, for a self-exchange reaction is given by $\lambda/4$, where λ is the reorganization energy associated with the reaction:

$$\mathrm{M_A} + \mathrm{M_B}^- = \mathrm{M_A}^- + \mathrm{M_B}$$

The reorganization energy (λ) can be separated into the sum of two primary components: (i) the medium reorganization energy that arises from modifications to the polarization of the surrounding medium due to the presence of excess charge (λ_s) and (ii) the intramolecular reorganization energy (λ_i), which combines the relaxation energies of the electron-donor molecule (λ_1) and electron-acceptor molecule (λ_2) associated with the electron-transfer reaction. We calculated the intramolecular contribution to the total reorganization energy for electron transfer and the corresponding value for hole transfer from the adiabatic potential surfaces for siloles **I**−**V**; the results are compared in Table 3. The total reorganization energies for electron transfer are ca. 0.5 eV, values comparable with those previously obtained for **1** and **2** at the same level of theory,[31] while those for hole transfer are in the range 0.4−0.6 eV. The reorganization energy values for electron transfer are approximately twice that calculated at the same level for $Alq_3^{0/-}$,[36] while those for hole transfer are approximately four to five times those calculated for $[pentacene]^{+/0}$ [37] and nearly twice those calculated for $TPD^{+/0}$.[38,39] Thus, the differences in electron mobilities that have been seen between siloles and Alq_3 are likely to be due to differences in intermolecular orbital overlap or to morphological effects (such as trapping at grain bound-

(33) Marcus, R. A. *J. Chem. Phys.* **1956**, *24*, 966.
(34) Barbara, P. F.; Meyer, T. J.; Ratner, M. A. *J. Phys. Chem.* **1996**, *100*, 13148−13168.
(35) Brédas, J. L.; Beljonne, D.; Coropceanu, V.; Cornil, J. *Chem. Rev.* **2004**, *104*, 4971−5003.
(36) Lin, B. C.; Cheng, C. P.; You, Z.-Q.; Hsu, C.-P. *J. Am. Chem. Soc.* **2005**, *127*, 66−67.
(37) Gruhn, N. E.; da Silva, D. A.; Bill, T. G.; Malagoli, M.; Coropceanu, V.; Kahn, A.; Brédas, J. L. *J. Am. Chem. Soc.* **2002**, *124*, 7918−7919.
(38) Malagoli, M.; Brédas, J. L. *Chem. Phys. Lett.* **2000**, *327*, 13−17.
(39) Lin, B. C.; Cheng, C. P.; Lao, Z. P. M. *J. Phys. Chem. A* **2003**, *107*, 5241−5251.

Table 4. Representative Vibrational Modes Corresponding to the Relaxation in the Neutral and Radical-Anion Potential Surfaces of **I′** (the Energy Value Represents the Contribution of Each Mode to the Total Relaxation Energy)

	neutral ω (cm^{-1})	S	energy (eV)	mode description
neutral	29	12.2	0.044	rotation of phenyl rings
	182	0.58	0.013	methyl−silicon−methyl bend
	947	0.12	0.014	ring breathing of silole & phenyl rings
	1536	0.20	0.038	ring breathing of silole & phenyl rings
	1550	0.40	0.077	ring breathing of silole & phenyl rings
anion	21	8.83	0.023	rotation of phenyl rings
	934	0.12	0.014	ring breathing of silole & phenyl rings
	1250	0.19	0.030	ring breathing of silole & phenyl rings
	1485	0.22	0.040	ring breathing of silole & phenyl rings
	1494	0.15	0.028	ring breathing of silole & phenyl rings
	1537	0.07	0.014	ring breathing of silole & phenyl rings
	1646	0.07	0.014	ring breathing of silole & phenyl rings

aries), rather than to differences in λ. The geometric modifications that occur on both reduction and oxidation of the silole systems are primarily localized toward the central portion of the molecular structures, particularly in the silole ring and in the exocyclic Si−Ar bonds, but also to some extent in some of the carbon−carbon bonds of the 2,5-phenyl rings in close proximity to the silole ring and in the torsional angle of the 2,5-phenyl rings with respect to the silole ring (see Tables S3 and S4 and Figure S1 in Supporting Information).[40] This localization is mainly responsible for the relatively large reorganization energy.

To gain further insight into the reorganization energy associated with the electron-exchange reaction between neutral and anionic siloles, we explored the contribution of different vibrational modes to the reorganization energy. Since the reorganization energies do not depend strongly upon the substituents on the silicon atom and since the geometric changes do not extend into this substituent, we investigated the simplest system, **I**; in addition, we also examined the model compound **I′**, in which the 3,4-phenyl groups are replaced by hydrogens, to reduce the number of degrees of freedom and simplify interpretation. The contribution of normal modes to the reorganization energy can be obtained through the relation:

$$\lambda_{\text{total}} = \sum \lambda_i = \sum S_i \hbar \omega_i$$

where S is the Huang−Rhys factor.[34,41] Normal-mode analysis for $\mathbf{I'}^{0/-}$ gives a value of 0.51 eV for λ, in good agreement with the value (0.47 eV) obtained from the adiabatic potential surfaces, and of similar magnitude to the values in Table 3 for **I**−**V**.[51] Five vibrational modes in $\mathbf{I'}^{0}$ within the neutral potential well comprise 73% of the total relaxation energy, as shown in Table 4. Of these five modes, three ring-breathing modes provide 51% of the total relaxation energy, while rotation of the phenyl rings with respect to the central silole ring makes up 17% of the total relaxation energy. Previous experimental evidence from a variety of techniques (solution fluorescence spectroscopy with variable temperatures and solvent viscosities, along with variable-temperature NMR experiments) suggests that such a rotational mode plays an important role in the intensity dampening of singlet emission for siloles in solution, and it is thought that restriction of such rotation is responsible for the aggregation-induced emission effects often observed for substituted silole molecules.[42,43] In the radical-anion potential well, 65% of the total relaxation energy is composed of six vibrational modes. The majority of the relaxation energy contribution (56%) comes from various ring-breathing mode combinations of the silole and phenyl rings, with significant contribution (9%) coming from phenyl-ring rotation with respect to the central silole ring. Thus, for this model system, the majority of the total intramolecular reorganization energy arises from combinations of ring-breathing modes of the central silole ring and the 2,5-susbtituted phenyl rings. Normal-mode analysis of $\mathbf{I}^{0/-}$ reveals a picture similar to that provided by $\mathbf{I'}^{0/-}$, though the complexity of the modes involved is much more significant due to the number of intrinsic degrees of freedom in the molecule. Again, λ obtained by the normal-mode analysis (0.50 eV) is close to that obtained via the adiabatic potential surface analysis (0.51 eV). Here, upward of 15 vibrational modes play significant roles in the relaxation processes on the neutral and radical-anion surfaces (see Supporting Information Table S5). As with $\mathbf{I'}^{0/-}$, the predominant vibrations consist of various ring-breathing modes and phenyl ring torsions, as well as Me−Si stretches/bends.

UV−Vis Absorption and Fluorescence Spectroscopy. Solution (chloroform) and thin-film UV−vis absorption spectra for the silole systems are shown in Figure 5, with the spectral characteristics summarized in Table 5. The lowest-energy maxima are essentially independent of the identity of the aryl group and little shifted between the solution and solid states, consistent with previous observations for other siloles.[44,45] TD-DFT calculations indicate that these transitions can be described as predominantly HOMO→LUMO in character (i.e., $\pi-\pi^*$ silacyclopentadiene transitions), but they somewhat underestimate the transition energies.[46]

Solution (chloroform) and thin-film PL spectra of the 1,1-substituted siloles **I**−**V** are shown in Figure 5, with emission data provided in Table 5. All five siloles show weak blue-green luminescence in solution, with very similar emission spectra peaked around 2.51−2.61 eV. Consistent with other siloles,[42,43] the fluorescence appears to be considerably brighter in the solid state relative to solution; however, the maxima are seen at similar energies (the features seen in the solid-state bands are slightly narrower, but this is presumably attributable to self-absorption).[47]

From the magnitude of the bulk transport gap E_t, also known as the single-particle gap, and the optical properties, one can estimate the solid-state exciton-binding energy (E_B). This is the energy required for photocharge generation of a silole anion and silole cation from an excited silole molecule (Frenkel

(40) These torsions are likely suppressed in the solid state.
(41) Pope, M.; Swenberg, C. E. *Electronic Processes in Organic Crystals and Polymers*, 2nd ed.; Oxford University Press: New York, 1999.
(42) Luo, J. D. et al. *Chem. Commun.* **2001**, 1740−1741.
(43) Chen, J. W.; Law, C. C. W.; Lam, J. W. Y.; Dong, Y. P.; Lo, S. M. F.; Williams, I. D.; Zhu, D. B.; Tang, B. Z. *Chem. Mater.* **2003**, *15*, 1535−1546.
(44) It should also be noted that spectra in nonpolar solvents (hexane or toluene) showed almost identical absorption maxima, as has been previously reported for other silole systems; see ref 10.
(45) We attribute the sharp absorption peaks in **III** to $\pi-\pi^*$ transitions within the fluorenyl groups.
(46) The calculations do not successfully reproduce the slight variations in absorption maxima between the compounds; in particular, the experimental maximum for the pentafluorophenyl derivative, **V**, is slightly red-shifted relative to that of the phenyl compound, **II**, but is calculated to be slightly blue-shifted. These differences may be due to experimental maxima being somewhat shifted from the vertical transition energies due to overlap with the tails of the higher energy (Ph and other aryl $\pi-\pi^*$) transitions.

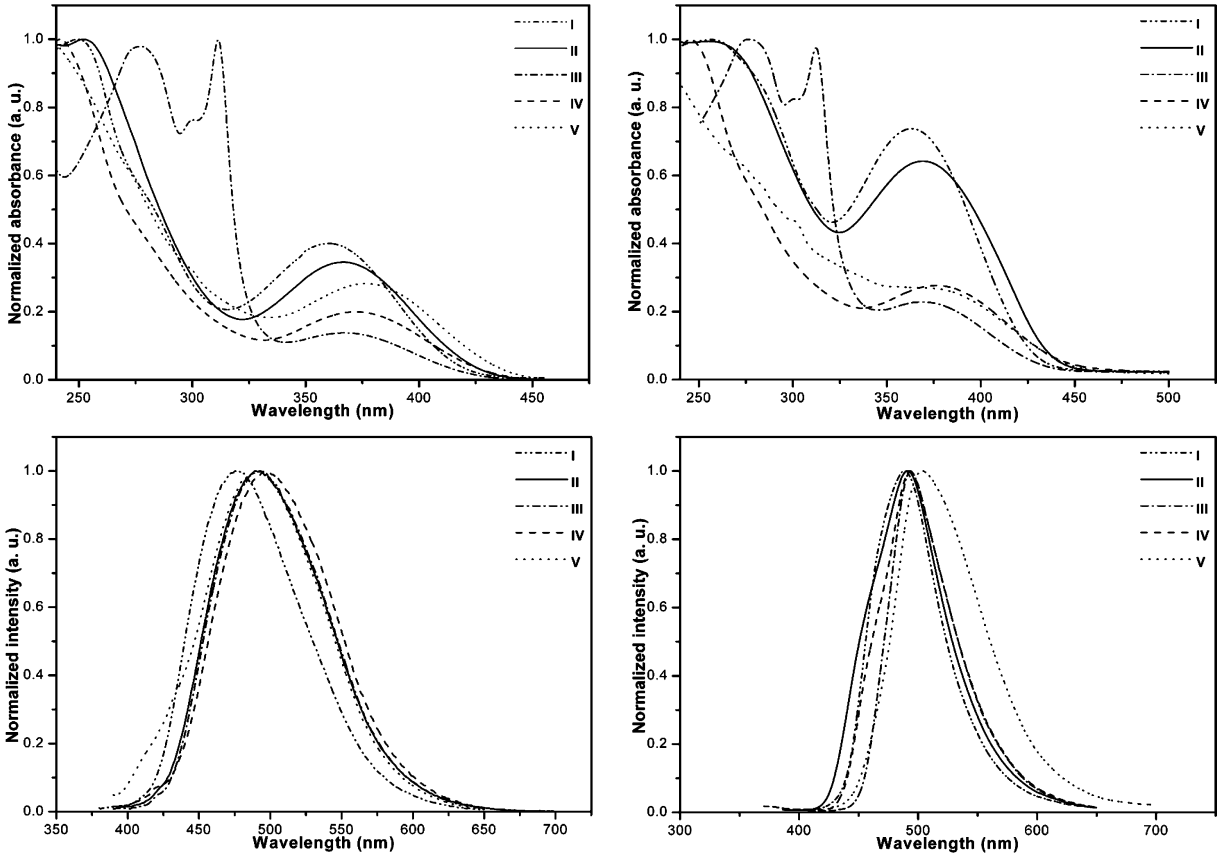

Figure 5. Solution (chloroform) (top left) and thin-film (top right) UV−vis absorption spectra and solution (chloroform) (bottom left) and thin-film (bottom right) fluorescence spectra of **I**−**V**.

Table 5. Experimental and TD-DFT Absorption and Experimental Emission Characteristics for the Lowest-Lying Excited States of **I**−**V**

	absorption (eV)[a]		emission (eV)[a]
	experiment	TD-DFT	
I	3.43 (3.41)	3.23	2.61 (2.54)
II	3.38 (3.36)	3.10	2.54 (2.53)
III	3.37 (3.38)	3.08	2.53 (2.51)
IV	3.33 (3.31)	3.05	2.51 (2.52)
V	3.30 (3.28)	3.14	2.53 (2.46)

[a] Measured in chloroform; data in thin films are given in the parentheses.

exciton), that is, the energy required for the reaction:

$$M^* + M = M^+ + M^-$$

which is given by:

$$E_B = E_t - E_{op}$$

where E_{op} is the 0−0 maximum. We evaluated E_t using a procedure previously established by Hill et al.[48] E_t is taken as the experimental peak-to-peak HOMO-to-LUMO gap measured by PES and IPES, reduced by 0.8 eV to account for: (i) the increase in polarization from surface to bulk (0.3 eV for the hole states and 0.3 eV for the electron states) and (ii) the loss of energy of the photoemitted electron (PES) and injected electron (IPES) to molecular vibration (2 × 0.1 eV; i.e., providing an approximate correction from vertical to adiabatic values). The experimental values shown in Table 6 indicate exciton-binding energies in the range 1.0−1.7 eV when E_{op} is estimated from the absorption maximum, similar to those estimated by the same method for other organic systems.[48,49] Values obtained from the DFT adiabatic surface energies and from TD-DFT absorption energies are much larger (ca. 2 eV),

Table 6. Exciton-Binding Energies as Determined by PES/IPES and DFT Calculated Ionization Potentials and Electron Affinities, and Solid-State UV/Vis and TD-DFT Absorption Data

method		IP (eV)	EA (eV)[a]	E_{op} (eV)[b]	E_t (eV)[c]	E_B (eV)
PES/IPES	**I**	–	–		–	–
	II	6.19	−1.85	2.97 *3.36*	4.54	1.57 *1.18*
	III	6.40	−1.49	2.94 *3.38*	5.11	2.17 *1.73*
	IV	6.05	−1.93	2.94 *3.31*	4.32	1.38 *1.01*
	V	6.78	−2.41	2.91 *3.28*	4.57	1.66 *1.29*
DFT/TD-DFT	**I**	6.30	−0.62	3.23	5.88	2.65
	II	6.19	−0.78	3.10	5.0	1.90
	III	6.10	−0.83	3.09	5.9	2.81
	IV	6.23	−0.85	3.04	4.6	1.56
	V	6.49	−1.16	3.14	5.25	2.11

[a] Note that the electron affinities are calculated by subtracting the total energy on the neutral electronic configuration from the energy of the radical-anion electronic configuration. [b] Experimental values for E_{op} estimated from the midpoint of absorption and fluorescence and from the absorption maxima (italics), for direct comparison with the DFT/TD-DFT results. [c] Experimental values of the transport gap are obtained as explained in the text.

(47) The fact that strong luminescence is observed in the solid state, along with minimal shifts in the luminescence energy, is consistent with previous reports for siloles. These results are in contrast to "typical" organic emitters that tend to undergo various degrees of aggregation and excimer formation that leads to concentration-dependent electroluminescence quenching, emission band broadening, and bathochromic shifts. The fact that siloles do not undergo these processes has been explained by the quenching of nonradiative decay routes in the solid state; see ref 14.

(48) Hill, I.; Kahn, A.; Soos, Z.; Pascal, R. *Chem. Phys. Lett.* **2000**, *327*, 181−188.

(49) Knupfer, M. *Appl. Phys. A* **2003**, *77*, 623−626.

though with a similar variation in energy across the series (0.25 eV); the discrepancy between experimental and DFT estimates of E_B can be attributed at least partly to the neglect in the DFT approach of the solid-state polarization effects that stabilize both cations and anions relative to the gas phase.

IV. Conclusion

We have measured the solid-state EAs of siloles using IPES; these are the most direct measurements to date of these important parameters for gauging their compatibility with other organic electronic materials and with inorganic electrode materials. Of the functional groups we have examined, only the very strongly electron-withdrawing pentafluorophenyl groups have a significant effect on the IP and EA. The variations in the EA and IP of 1,1-diaryl-2,3,4,5-tetraphenylsiloles with the identity of the aryl groups, Ar, appear to be largely dictated by inductive effects. This conclusion is also supported by DFT calculations. Thus, thiophene, despite having an electron-rich π-system, acts as a weakly electron-withdrawing group on the silole skeleton when attached to the silicon atom. Another result of the inductive role played by the Ar group is that the HOMO−LUMO gap and, hence, the optical absorption or fluorescence properties are rather insensitive to the identity of Ar.

Since EA measurements of ET materials are scarce, many workers have estimated EA from electrochemical data, often using the known IP or EA of a reference material.[50] We have shown here that estimates of the EAs of siloles from electrochemical data are only in good agreement with the IPES values if one uses another ET material of known EA, such as Alq_3, as a reference material; estimates based on the known IP of TPD lead to overestimation of the magnitude of the EAs by more than 1 eV. Estimates of EA based on IP and optical data are also poor since they neglect the exciton-binding energy.

We have also used DFT to calculate the reorganization energy associated with the electron-transfer reactions of siloles and their radical cations or anions. These reorganization energies are somewhat larger than those for Alq_3, suggesting that this is not the factor determining the higher electron mobilities reported in siloles. From optical data and the transport gap deduced from PES and IPES data, we have been able to estimate exciton-binding energies for siloles. Finally, the similarity of the EAs we have measured to that of the widely used Alq_3, combined with the high electron mobilities previously reported for other siloles, suggests that these materials could potentially replace Alq_3 in many ET applications; the C_6F_5 derivative, which has the lowest-lying LUMO and, therefore, the lowest barrier to electron injection, is particularly promising.

Acknowledgment. This material is based upon work supported in part by the National Science Foundation STC Program under Agreement No. DMR-0120967. We also thank the NSF for support through Grants DMR-0408589, CHE-0342321, and CHE-0211419 and the Office of Naval Research for support through a MURI (Award No. N00014-03-1-0793, administered through the California Institute of Technology). Support from Georgia Institute of Technology, through the Center for Organic Photonics and Electronics, from the New Jersey Center for Organic Optoelectronics, and from the Princeton Institute for the Science and Technology of Materials is also gratefully acknowledged.

Supporting Information Available: Tables of thermal data for **I**−**V**; calculated frontier orbital energies for **I**−**V**; calculated geometric parameters for **I**−**V** in neutral, anionic, and cationic states; calculated vibrational modes associated with the relaxation in neutral and anionic surfaces of **I**. Complete citations for refs 23, 25, and 42. This material is available free of charge via the Internet at http://pubs.acs.org.

JA051139I

(50) Domercq, B.; Grasso, C.; Maldonado, J. L.; Halik, M.; Barlow, S.; Marder, S. R.; Kippelen, B. *J. Phys. Chem. B* **2004**, *108*, 8647−8651.
(51) Analysis of the vibrational mode contribution to the intramolecular reorganization energy was carried out with the DUSHIN program of J. R. Reimers (Reimers, J. R. *J. Chem. Phys.* **2001**, *115*, 9103).